Modelling and Control System Design for Doubly-Fed Induction Generator Based Wind Turbines

*Melikşah ÖZAKTÜRK
*Faculty of Engineering and Architecture, Department of Electrical and Electronics Engineering,
Eskisehir Osmangazi University, Turkey

Abstract

Wind turbine modelling using doubly-fed induction generators is a well-known subject. However studies have tended to focus on optimising each component of the system rather than considering the system as a whole. This paper proposes the control methods for doubly-fed induction generator (DFIG) based wind turbine applications and as well as includes modelling of the DFIG. The control designs of inner and outer loops of rotor-side and grid-side converters of the DFIG model are both well established and shown to work. The DFIG system is simulated in PSCAD software programme and the simulation results are validated against mathematical analyses.

Key words: DFIG, rotor-side, grid-side, modelling, converter control.

1. Introduction

Wind power today has an increasing importance in power production. Investments in wind energy technologies have been continuously made to generate clean and environmental friendly energy. Apart from construction and decommissioning, these systems never emit carbon dioxide (CO_2) to the atmosphere. However, one of the main disadvantages of using wind power is that the wind speed is unpredictable and very changeable. To alleviate the effect of this drawback, doubly-fed induction generators (DFIGs), which can operate at variable speeds, are widely used in wind power conversion applications to maximise power generation and to reduce acoustic noise, converter costs and mechanical loads onto the nacelle [1, 2 and 3]. Hence, DFIG wind turbines currently dominate the market due to their cost-effective provision of variable-speed operation [1].

The control of a DFIG is more complicated than that of a standard induction machine. Integrating the various subsystem controllers is also challenging. Aspects of system control have been extensively discussed. As an example, a rotor-side converter control of a DFIG is investigated in [4] while a control design for the grid-side converter is proposed in [5]. However, the difficulty to date is that each component has largely been considered individually not as part of a larger or whole system. This paper considers all significant electrical components of a typical DFIG wind turbine system in order to try to model and control the system as a whole. Turbine mechanical dynamics and blade pitching control are excluded, since these present a slower set of dynamics, which are considered to be out of interest of this paper.

*Corresponding author: Address: Faculty of Engineering and Architecture, Department of Electrical and Electronics Engineering, Eskisehir Osmangazi University, 26480, Eskisehir, TURKEY. E-mail address: ozakturk@ogu.edu.tr

2. Doubly-Fed Induction Generator (DFIG) Modelling

The main electrical components of a DFIG wind turbine are a back-to-back converter, i.e. a rotor-side and a grid-side converter, a DC-link capacitor placed between these two converters, and protection of power electronic components, e.g. a rotor crowbar or/and a DC-link brake (See Figure 1). As seen in Figure 1, the DFIG is connected to the grid via a transformer while its rotor windings are connected to the rotor-side converter via slip rings.

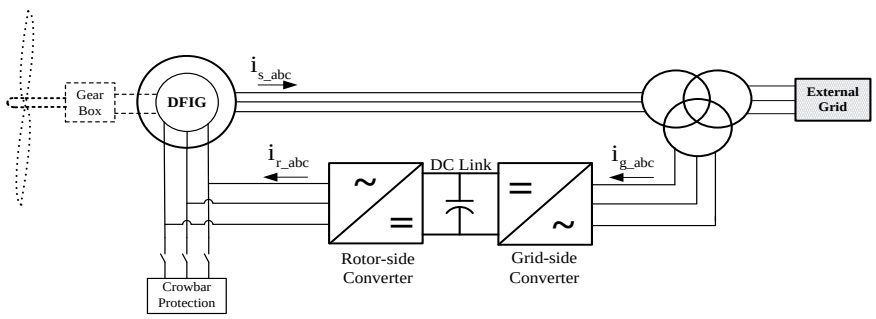

Figure 1: Typical DFIG-based wind turbine system

The dynamic machine equations in the excitation reference frame are well known, for a wound rotor induction machine in which the stator windings connect to a stiff voltage supply while the rotor windings connect to a bi-directional power converter. Full machine equations and related assumptions made can be seen in [4]. The machine equations of stator active and reactive power are as follows:

$$P_s = -(3V_s L_m i^e_{r\_q} \big/ \sqrt{2} L_{ss}) \tag{1}$$

$$Q_s = (3V_s \big/ \sqrt{2} L_{ss})(\Psi^e_s - L_m i^e_{r\_d}) \tag{2}$$

In Equation 1, the negative stator active power means that the direction of the active power is from the machine to the grid (generation mode). If Equation 2 results in a positive stator reactive power, this means that there is a lagging stator power factor existing which can be compensated with the *d*-component of the rotor current. Thus, the inductive power flows from the grid to the machine as excitation power. A negative stator reactive power indicates a leading stator power factor though. Equations 1 and 2 show that there is a linear relationship between the *q*-component of the rotor current and the stator real power whereas the stator reactive power is a function of the *d*-component of the rotor current in case the stator voltage and the stator flux stay constant. In other words, the stator active power can be controlled by the *q*-component of the rotor current while the stator reactive power can be regulated by the *d*-component of the rotor current. The machine equation of the rotor voltage in the excitation frame (e-frame) is:

$$\bar{v}^e_r = R_r \bar{i}^e_r + L_c p \bar{i}^e_r + kp\bar{\Psi}^e_s + j\omega_{slip} L_c \bar{i}^e_r + kj\omega_{slip}\bar{\Psi}^e_s \tag{3}$$

where $\omega_{slip} = \omega_s - \omega_r$, $L_c = L_{rr} - (L_m^2 \big/ L_{ss})$, $k = L_m \big/ L_{ss}$ *and* $p = d/dt$

3. Rotor-side Converter (RSC) Control

The main function of the RSC is to control the real and reactive power of the DFIG by controlling the *dq*-components of the rotor currents. The RSC also provides the required magnetisation power to the generator through the rotor circuit. The RSC control is constituted by two cascaded-controls, namely the current (inner) loop control and the power (outer) loop control. Both of these controllers should be designed and tuned accurately in order to maintain a good control of the RSC, which directly influences the quality of the power.

3.1. RSC Inner (Current) Loop Control

The current (inner) loop control of the RSC can be designed by splitting the rotor voltage equation given in Equation 3 into *dq*-components in terms of generation convention and by neglecting the stator flux transients (in steady-state $d\Psi_s/dt=0$) gives:

$$v^*_{r\_d} = R_r i_{r\_d} + L_c p i_{r\_d} - \omega_{slip} L_c i_{r\_q} \tag{4}$$

$$v^*_{r\_q} = R_r i_{r\_q} + L_c p i_{r\_q} + \omega_{slip} L_c i_{r\_d} + \omega_{slip} k \Psi_{s\_d} \tag{5}$$

Equations 4 and 5 are utilised in order to create the current loop control of the RSC. The block diagram of the decoupled inner loop control of the RSC is depicted in Figure 2. A standard PI controller is used since it is adequate to control both the damping and the bandwidth due to the nature of the inner plant.

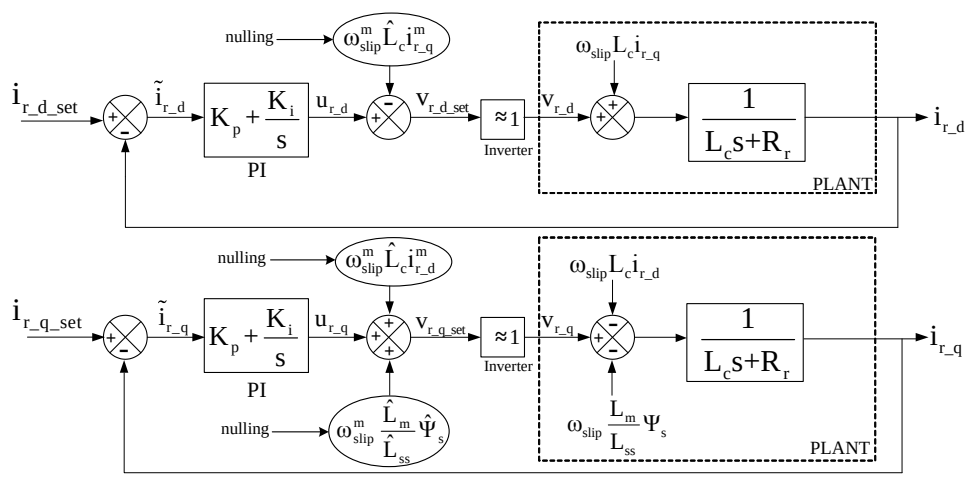

Figure 2: Decoupled current (inner) loop control of RSC

As seen in Figure 2, the cross coupling term in the *d*-loop and those in the *q*-loop are nulled. By nulling the coupling terms, the effects of *d*-components onto the *q*-loop current (inner) control and those of *q*-components onto the *d*-loop current control would then be eliminated. Thus, fast control of the RSC inner loop can be achieved. However, the reliance on the exact parameter

knowledge of nulled quantities is unavoidable. The effectiveness of this nulling method is also subject to the accurate measurement of parameters, errors and noise.

In case of small disturbances, the errors of not nulling could be ignored as there should be a little influence of the disturbance on the control response. The corollary of this is that there need not be 100% accurate nulling control though. In any case complete nulling is only theoretically possible but not practically achievable.

3.2. RSC Outer (Power) Loop Control

The conventional control approach for DFIG converters is to use a PI control. Using a PI controller for the outer (power) loop control of the RSC gives a first-order transfer function due to the nature of the outer plant considered in this research. In this case, the PI controller allows setting only the bandwidth but unfortunately not the damping. Therefore, in order to be able to set both the bandwidth and the damping, the PI controller is replaced with a PID controller. However, the tuning process of the PID controller is more complicated than that of the PI controller, and selecting of the PID tuning parameters should be done very carefully. Neglecting the inner loop of the RSC by assuming that it is fast ($G_{inner}\approx 1$), the outer loop control block diagram can be depicted as in Figure 3 by utilising Equations 1 and 2.

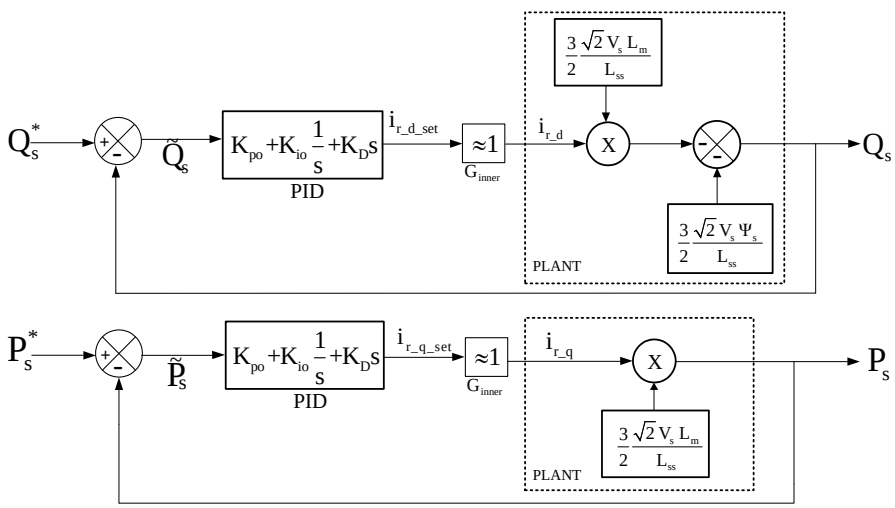

Figure 3: Outer (power) loop control of RSC utilising the PID controller

4. Grid-side Converter (GSC) Control

The significant role of a GSC used in variable speed wind turbine systems is primarily to keep the DC-link voltage constant at a pre-set value. This is maintained by a DC-link capacitance. Additionally, a GSC conveys the rotor power to or from the network as well. A typical grid-side converter arrangement is illustrated in Figure 4.

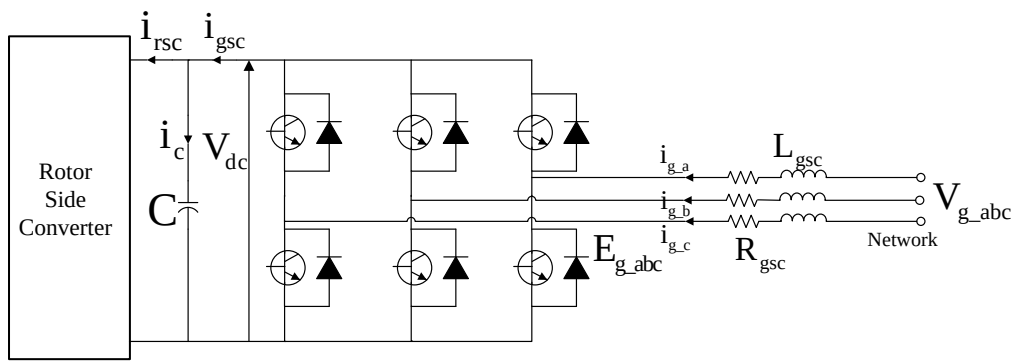

Figure 4: Grid-side converter configuration

The voltage balance across the inductor, L_{gsc}, is:

$$\begin{aligned} v_{g\_a} &= R_{gsc} i_{g\_a} + L_{gsc} p i_{g\_a} + e_{g\_a} \\ v_{g\_b} &= R_{gsc} i_{g\_b} + L_{gsc} p i_{g\_b} + e_{g\_b} \\ v_{g\_c} &= R_{gsc} i_{g\_c} + L_{gsc} p i_{g\_c} + e_{g\_c} \end{aligned} \tag{6}$$

where L_{gsc} and R_{gsc} are the coupling inductance and resistance to the grid, respectively.

Using the *abc* to $\alpha\beta$ (Clarke) and then $\alpha\beta$ to *dq* (Park) transformations, and resolving the partial differentials, Equation 6 turns into a *dq* reference frame rotating at ω_e (in the case considered in this work, ω_e is chosen as the supply angular frequency, ω_s):

$$v_{g\_d} = R_{gsc} i_{g\_d} + L_{gsc} p i_{g\_d} - \omega_e L_{gsc} i_{g\_q} + e_{g\_d} \tag{7}$$

$$v_{g\_q} = R_{gsc} i_{g\_q} + L_{gsc} p i_{g\_q} + \omega_e L_{gsc} i_{g\_d} + e_{g\_q} \tag{8}$$

4.1. GSC Inner (Current) Loop Control

The inner (current) loop control block diagram of the GSC is drawn by the use of Equations 7 and 8. The terms of $\omega_s L_{gsc} i_{g\_q}$ and $\omega_s L_{gsc} i_{g\_d}$ in the physical plant are nulled by adding the control signals of $\omega_s^m \hat{L}_{gsc} i_{g\_q}^m$ and $\omega_s^m \hat{L}_{gsc} i_{g\_d}^m$, respectively, to the output of the PI controller, since the polarity of the PI output is negative. Additionally, in the same manner v_{g_d} and v_{g_q} components are also nulled to eliminate their effects on the inner loop control (see Figure 5).

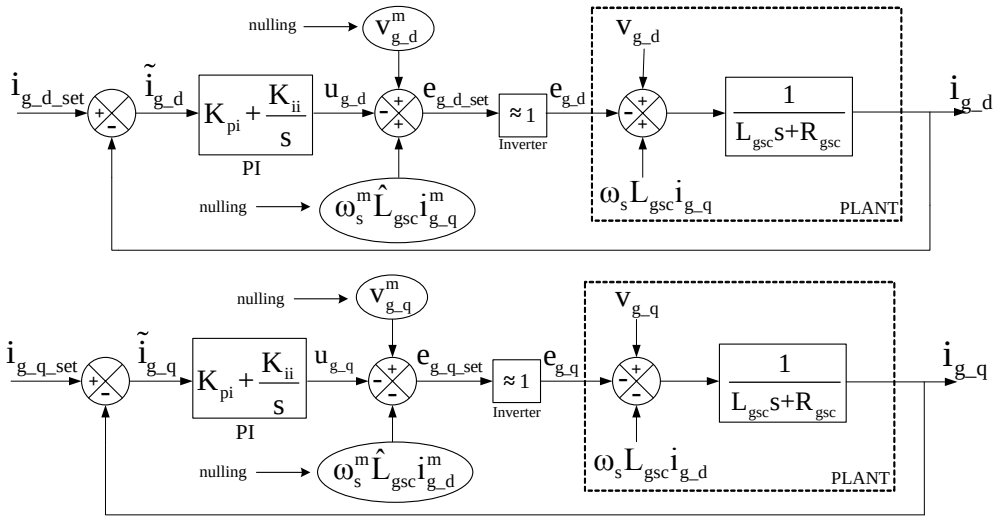

Figure 5: Decoupled inner (current) loop control of GSC

4.2. GSC Outer Loop Control (DC-link Voltage Control)

The grid-side converter shown in Figure 1 can be represented as the DC-link voltage plant, which is illustrated in Figure 6, in order to derive the outer (voltage) loop plant model and to design the control of the outer loop of the GSC [6]. The grid voltage is aligned to the *d*-axis, so the *q*-components of the voltage and current quantities are zero, i.e. v_{g_q}=0 and i_{g_q}=0.

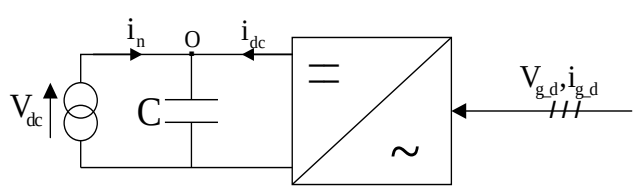

Figure 6: DC-link voltage plant

Many physical phenomena in the real word have nonlinear characteristics, but it is often nearly impossible to mathematically model and analyse these systems. Therefore, a small-signal linearisation technique is often used to ease the modelling of non-linear systems by representing them as linear systems within a target operating point range. Thus, a stable system within the limited operating region would be maintained and the controller design for non-linear systems can then be made possible. However, the linearised system will include components which vary with some state variables (i.e. with operating points) [7]. In this paper, a small signal linearisation method is utilised to extract the plant model of the outer loop and to design its controller.

Applying the Kirchhoff's Current Law to node ‘O’ in Figure 6:

$$pV_{dc}C = i_n + i_{dc} \tag{9}$$

Using the power invariant principle for the DC-end and AC-end ($P_{DC} = P_{AC}$):

$$P_{DC} = v_{dc}i_{dc} \text{ and } P_{AC} = 3/2(v_{g\_d}i_{g\_d}) \Rightarrow v_{dc}i_{dc} = 3/2(v_{g\_d}i_{g\_d}) \tag{10}$$

gives the DC-voltage term as:

$$pV_{dc} = (i_n/C) + (3v_{g\_d}i_{g\_d}/2CV_{dc}) = f \tag{11}$$

Taking partial differentials and ignoring all terms apart from the noise term, the direct current the DC-voltage terms turn the equation into:

$$\begin{aligned}\Delta\dot{V}_{dc} &= \frac{\partial f}{\partial i_n}\Delta i_n + \frac{\partial f}{\partial v_{dc}}\Delta v_{dc} + \frac{\partial f}{\partial i_{g\_d}}\Delta i_{g\_d} + \frac{\partial f}{\partial v_{g\_d}}\Delta v_{g\_d} \\ &= \frac{\Delta i_n}{C} - \frac{3v_{g\_do}i_{g\_do}}{2C(v_{dco})^2}\Delta v_{dc} + \frac{3v_{g\_do}}{2Cv_{dco}}\Delta i_{g\_d} + \frac{3i_{g\_do}}{2Cv_{dco}}\Delta v_{g\_d} \\ or\ \ C\Delta\dot{V}_{dc} &= \Delta i_n - 1.5K_vK_s\Delta v_{dc} + 1.5K_v\Delta i_{g\_d} + 1.5K_s\Delta v_{g\_d}\end{aligned} \tag{12}$$

where a subscript 'o' indicates an operating point value, $K_v = v_{g\_do}/v_{dc\_o}$ and $K_s = i_{g\_do}/v_{dc\_o}$

Equation 12 yields the outer (voltage) loop plant model of the GSC that is used to design outer loop control. Assuming that the inner (current) loop is far faster than the outer (voltage) loop of the GSC ($G_{inner}\approx 1$), the outer loop control block diagram of the GSC can then be depicted as seen in Figure 7.

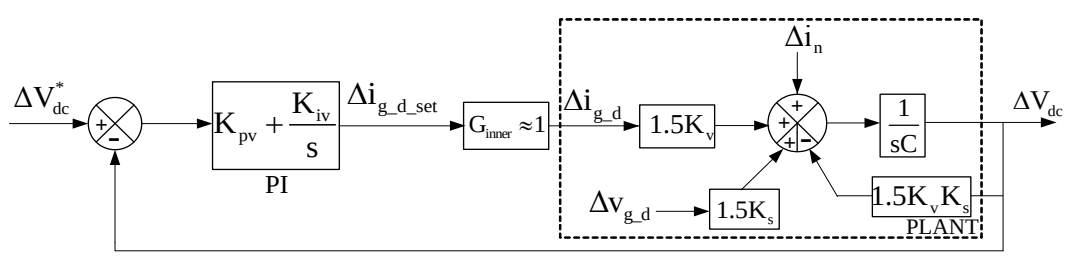

Figure 7: Outer (V_{dc}) loop control of the grid-side converter

5. Simulation Results

The simulation results are obtained by running the DFIG system model in PSCAD with a fixed over-synchronous speed (generating mode) of 1.05pu. The reference values of the stator real, reactive power and the DC-link voltage are set to -1MW, -1MVAr and 1kV, respectively.

In order to verify the relationship between the stator active and reactive power and the *dq*-components of the rotor currents given in Equations 1 and 2, the small-step changes are applied to the reference values of the powers in turn, while keeping one of them constant at its pre-set value at every turn (see Figure 8).

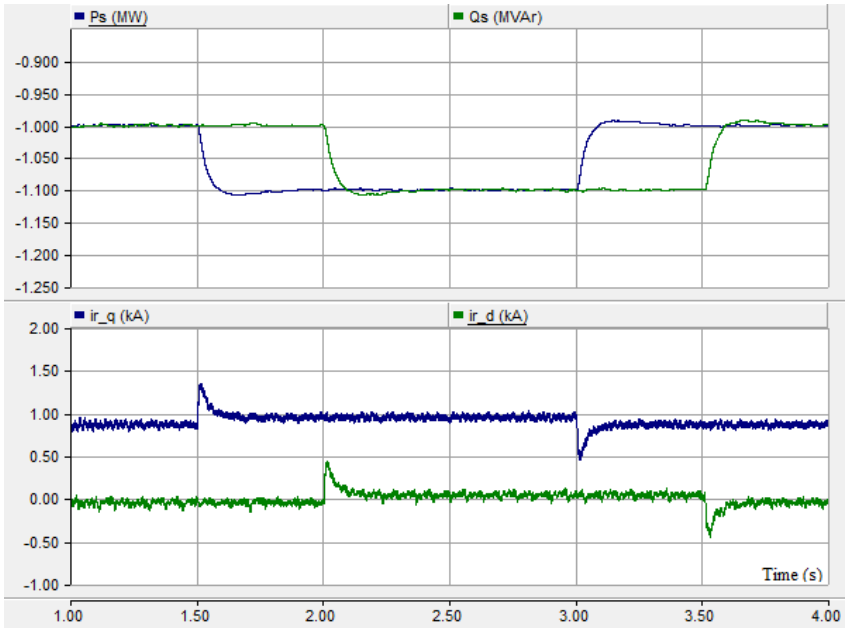

Figure 8: The relationships between the rotor currents, and the stator active and reactive power

In Figure 8, as long as the stator active power varies, only the *q*-component of the rotor current changes, while the change in the stator reactive power causes a change in only the *d*-component of the rotor current. Figure 8 confirms that the simulation results are consistent with the mathematical analyses. Furthermore, the waveforms of the stator active and reactive power step responses are shown to be effectively same in Figure 9.

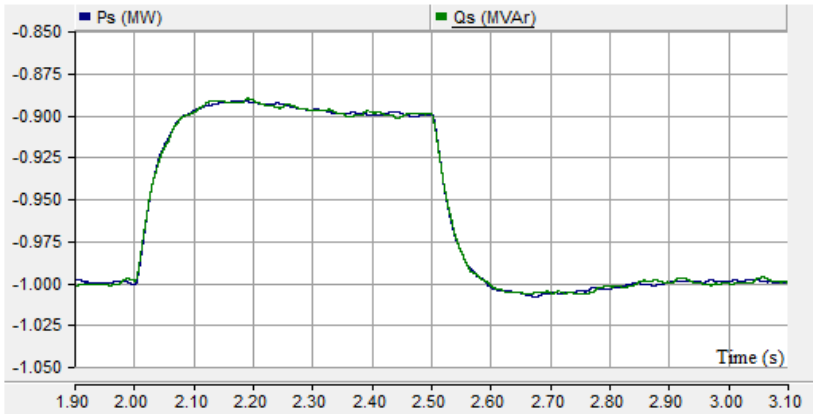

Figure 9: The waveforms of the stator active and reactive power

The simulation results presented in Figures 8 and 9 tell that the control design for the RSC works accurately. The control design of the GSC is also evaluated by applying step changes in the DC-link voltage. Due to the power invariant principle, the power at the AC-end is equal to the power at the DC-end (see Equation 10). A direct proportional relationship between the DC-link voltage and the *d*-component of the grid-side current (i_{g_d}), where the *d*-component of the grid-side voltage (v_{g_d}) is constant, is given in Equation 10. There is also a direct relation between the *d*-component of the grid-side current (i_{g_d}) and the grid-side real power (AC-end real power). Therefore, an indirect relationship between the DC-link voltage and the grid-side real power occurs. These mathematical interrelationships are verified and supported by the simulation results demonstrated in Figure 10.

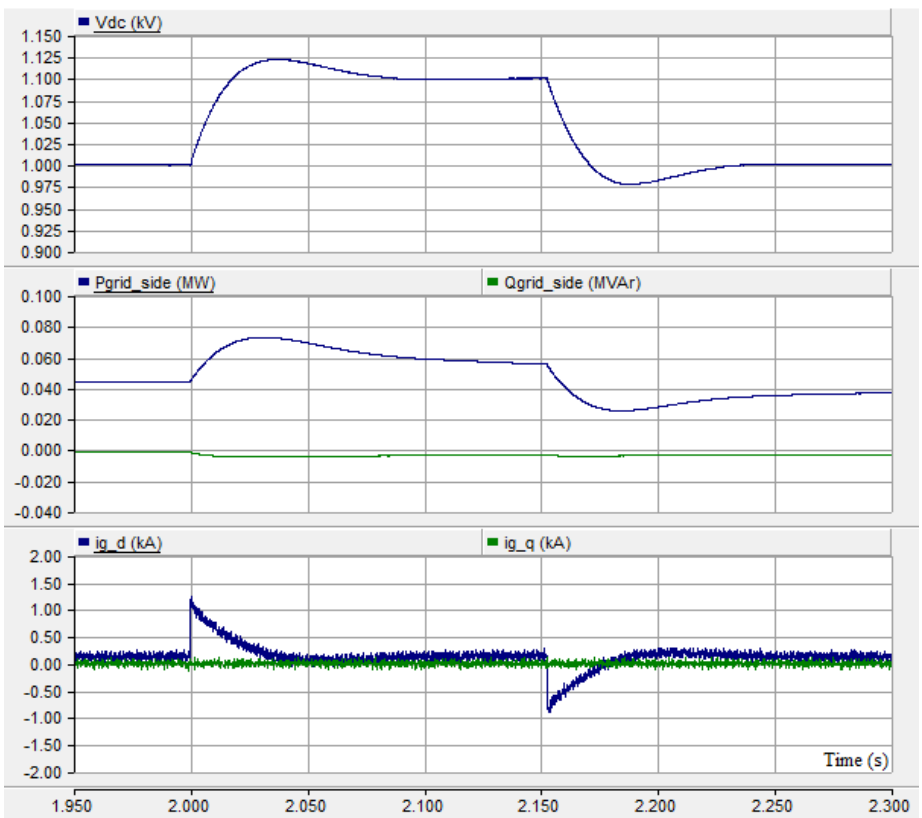

Figure 10: Simulation results of the GSC control

6. Conclusions

The DFIG modelling and its dynamic equations are briefly given. The control of the inner and outer loops of the RSC and GSC are designed and their control block diagrams are depicted. The DFIG system including its all electrical components is investigated as a whole system. The turbine aero-mechanical dynamics are excluded since these are out of interest in this paper. The control designs established for the rotor-side and grid-side converters of the DFIG based wind

turbine system are shown to work precisely. The mathematical equations of the DFIG model are justified by the simulation results.

Appendix

Parameters that are used in DFIG wind turbine are:

Electrical Generator Data		DC-link and Frequency Converters	
Rating	4.5 MVA	C_{base}	0.014324 F
Stator Voltage (L-L, RMS)	1 kV	C	3.5 pu
L_s	0.09241 pu	V_{dc}	1 kV
L_r	0.09955 pu	L_{gsc}	1 pu (per 0.4 kV base
L_m	3.95279 pu	R_{gsc}	0.017 pu (per 0.4 kV base)
R_s	0.00488 pu	L_{rsc}	0.2 pu (per 1 kV base)
R_r	0.00549 pu	R_{rsc}	0 pu (per 1 kV base)

Acknowledgement

The author would like to thank the Ministry of National Education of Republic of Turkey for their financial support during his PhD study at University of Manchester, UK.

References

[1] Hansen AD, F. Lov, Blaabjerg F, Hansen LH. Review of contemporary wind turbine concepts and their market penetration. Wind Engineering 2004;28:247-263.
[2] Burton T, Sharpe D, Jenkins N, Bossanyi E. Wind energy handbook. UK:John Wiley and Sons Ltd.;2001.
[3] http://www.wind-energy-the-facts.org/en/downloads.html. Wind energy - The facts, volumes 1 and 2, coordinated by the European Wind Energy Association (EWEA). Accessed on 15th March 2013.
[4] Hopfensperger B, Atkinson D, Lakin R. Stator-flux-oriented control of a doubly fed induction machine with and without position encoder. IEE Proceedings - Electric power applications 2000;147:241-250.
[5] Pena R, Clare JC, Asher GM. Doubly fed induction generator using back-to-back PWM converters and its application to variable speed wind-energy generation. IEE Proceedings - Electric power applications 1996;143:231-241.
[6] Barnes M. MSc Notes. University of Manchester. UK;2010.
[7] Golnaraghi F, Kuo BC,. Automatic control systems. 9th ed. John Wiley & Sons, Inc.;2010.